# Multiphoton absorption and Rabi oscillations in armchair graphene nanoribbons

B. S. Monozon[1] and P. Schmelcher[2,3]

[1]*Physics Department, Marine Technical University, 3 Lotsmanskaya Street, 190121 St.Petersburg, Russia*

[2]*Zentrum für Optische Quantentechnologien, Universität Hamburg, Luruper Chaussee 149, 22761 Hamburg, Germany*

[3]*The Hamburg Centre for Ultrafast Imaging, Universität Hamburg, Luruper Chaussee 149, 22761 Hamburg, Germany*

(Received 11 January 2022; accepted 16 March 2022; published 31 March 2022)

We present an analytical approach to the problem of the multiphoton absorption and Rabi oscillations in an armchair graphene nanoribbon (AGNR) in the presence of a time-oscillating strong electric field induced by a light wave directed parallel to the ribbon axis. The two-dimensional Dirac equation for the massless electron subject to the ribbon confinement is employed. In the resonant approximation the electron-hole pair production rate, associated with the electron transitions between the valence and conduction size-quantized subbands, the corresponding multiphoton absorption coefficient, and the frequency of the Rabi oscillations are obtained in an explicit form. We trace the dependencies of the above quantities on the ribbon width and electric field strength for both the multiphoton assisted and tunneling regimes relevant to the time-oscillating and practically constant electric field, respectively. A significant enhancement effect of the oscillating character of the electric field on the intersubband transitions is encountered. Our analytical results are in qualitative agreement with those obtained for the graphene layer by numerical methods. Estimates of the expected experimental values for the typically employed AGNR and laser parameters show that both the Rabi oscillations and multiphoton absorption are accessible in the laboratory. The data relevant to the intersubband tunneling makes the AGNR a one-dimensional condensed matter analog in which the quantum electrodynamic vacuum decay can be detected by applying an external laboratory electric field.

DOI: 10.1103/PhysRevB.105.115435

## I. INTRODUCTION

The pioneering work by Wallace [1] devoted to the electron states in graphene, an ideal two-dimensional (2D) crystal of carbon atoms arranged on a honeycomb lattice, has lead to a series of experimental and theoretical investigations resulting in a vast literature (see Refs. [2,3] and references therein). This undiminished interest is caused by its unique mechanical, electronic, optical, and transport properties [4], which in turn is the consequence of the graphene electron nature. In the vicinity of the $\vec{K}^{\pm}$ corners of the graphene Brillouin zone (corresponding to Dirac points) the electron dispersion law looks like $\varepsilon = \hbar v_F k$, where $\varepsilon$ and $\vec{k}$ are the energy and 2D wave vector, respectively, counted from the Dirac points, where $v_F = 10^6$ m/s is the graphene Fermi velocity. This linear law results in the low energy electron states to be governed by a massless 2D Dirac equation [1,2]. The numerous branches of graphene studies might be grouped into two classes. The first one is investigations contributing to corresponding applications (phase modulators, nanopore sensors, ballistic transistors photodetectors, topological insulators [5]), and fundamental science (Klein tunneling, Zitterbewegung, quantum Hall effect), both related to condensed matter physics. In the second class of works graphene plays the role of a physical environment, in which some of the basic quantum electrodynamic (QED) effects, predicted earlier, can be verified in a laboratory. The existing experimental facilities prevent these effects to be observed in vacuum. The linear dispersion law for the massless fermions up to the energy $\varepsilon \simeq 1$ eV allow us to consider graphene as a condensed matter counterpart for relativistic quantum field theory and a filled Fermi sea in graphene as a filled Dirac sea in QED vacuum [6].

The vacuum decay in the presence of a strong classical electromagnetic field, accompanied by the electron-positron pair production (pp), remains one of the most important QED effects. Originally, it has been predicted by Sauter [7] in the context of the Klein paradox [8], firmly theoretically described by Schwinger [9], commented by Nikishov [10] and Cohen and McGady [11], and investigated by the $S$-matrix [12,13] and quasiclassical [14,15] methods (see Ref. [16] for details) to give for the pp rate

$$W^v \sim \exp\left(-\frac{\pi F_c^v}{F}\right). \tag{1}$$

In Eq. (1) $F$ and $F_c^v = \frac{m^2c^3}{e\hbar}$ are the time-independent external and critical electric fields, respectively. The latter provides the balance between the energy an electron acquires for the Compton wavelength and a gap $2mc^2$ in the vacuum energy spectrum. The experimental observation of the Schwinger vacuum decay is challenged by the extremely strong critical field $F_c^v \simeq 10^{13}$ kV/cm, which considerably exceeds the currently highest possible experimental values $F_{\text{expt}} \simeq 10^{-2}F_c^v$ [17], which leads to the exponential suppression of the pp rate $W^v$.

 

In the case of a time-oscillating electric field of magnitude $F_0$ and frequency $\omega$, the particle-field interaction in vacuum is determined by the Keldysh parameter [18]

$$\gamma^{(v)} = \frac{\omega mc}{eF_0}, \tag{2}$$

distinguishing the Schwinger interband tunneling ($\gamma^{(v)} \ll 1$) and multiphoton assisted ($\gamma^{(v)} \geqslant 1$) mechanisms of the pp. The exact equations for the numbers of fermion and boson pairs, created from the vacuum by the time-periodic electric field, have been derived by Mostepanenko and Frolov [19]. The enhancement of the pp output by the high frequency electric field was discussed in Refs. [20–25]. It is noteworthy that the multiphoton pp from the vacuum becomes insignificant for frequencies less than those in the gamma region [26,27]. The decay of the arbitrary dimensional QED, induced by the quasiconstant electric field, has been studied by Gavrilov and Gitman in Ref. [28], in which, in particular, the mean numbers of created bosons and fermions particles were determined. Recently Taya [29], based on the Dirac equation and Furry approach [30], comprehensively studied and thoroughly reviewed the problem of the interplay between the low frequency strong and fast oscillating perturbative electromagnetic fields. It was shown that such field interaction results in the significant growth of the electron-positron production from vacuum. In [31] the vacuum pp by a time-dependent strong electric field on the basis a semiclassical Wentzel-Kramers-Brillouin analysis has been explored.

In order to gain insight into the mechanisms of the vacuum decay accompanied by the electron-positron pp, the methods, relevant to the 3+1-dimensional QED vacuum, have been extended to the similar semiconductor structures and to the vacuum 2+1 analog, namely graphene layer, related to the electron-hole (e-h) pp. Linder *et al.* [32] employed the parallel between the Dirac and two-band equations for the electron-positron in vacuum and e-h pairs in the narrow-gapped semiconductors [33], respectively. The enhancement of the pair creation Landau-Zener probability [34,35], caused by the weak time-oscillating electric field superimposed on the strong constant [9] or slowly varying Sauter pulse [7] electric fields, has been discussed. Thus, the narrow-gapped semiconductors become the media for the laboratory testing of the fundamental quantum field theory predictions.

For a constant electric field the pp rate has been calculated both analytically and numerically for the gapless (massless) and gapped (massive) graphene [6,26,36,37]. In particular, Allor *et al.* [6] proposed an experimental test for the Schwinger tunneling mechanism. Effects of the time-dependent electric field on the pair creation in the gapped and gapless graphene have been investigated for periodically oscillating [36,38], different time pulses [5,39], and Sauter-like [7,26] electric fields. Recently, Akal *et al.* [17] studied dynamically assisted pp in gapped graphene monolayers subject to bichromatic electric fields. Gagnon *et al.* [40] investigated the dynamical pair creation in the presence of strong magnetic fields directed perpendicular to a graphene monolayer.

As it follows from the theoretical results of the works listed above, gapped graphene is suitable as a condensed matter emulator for the experimental test of the pp in vacuum, induced by the electric field. The point is that the electric fields, needed for the particle-antiparticle pair creation in graphene, can be realized in modern experimental laboratories in contrast to vacuum, for which the corresponding fields remain unattainable. The gapped graphene critical electric field $F_c^g$ can be obtained from $F_c^v$ in Eq. (1) by replacing $c$ by $v_F$ and $m$ by $\Delta_g/v_F^2$ where $\Delta_g$ is a band gap, induced, for example, by epitaxial growth on a suitable substrate [41]. For the realistic band gap $\Delta_g \simeq 0.3$ eV [41] the critical electric field is $F_c^g \simeq 1.6 \times 10^3$ kV/cm, which is much less than the vacuum field $F_c^v$.

For the time-oscillating electric field, the Keldysh parameter $\gamma^{(g)}$ is obtained from $\gamma^{(v)}$ in Eq. (2) by the same replacements as those associated with the field $F_c^g$. For the infrared electromagnetic wave ($\hbar\omega \simeq 0.1$ eV), providing the multiphoton mechanism of the pair creation ($\gamma^{(v)} = \gamma^{(g)} \simeq 1$, $\Delta_g \simeq 0.3$ eV), the field magnitudes for the vacuum and gapped graphene become $F_0^v \simeq 3 \times 10^6$ kV/cm and $F_0^g \simeq 5 \times 10^2$ kV/cm, respectively. The graphene related electric fields correspond to the laser intensity $I \simeq 6.5 \times 10^5$ kW/cm$^2$, which can be comfortably reached by present laser technology. In gapless graphene ($\Delta = 0$) the zero effective mass $m = 0$ ensures the pp for any electric fields and frequencies [38] and prevents the existence of a critical electric field and exponential suppression. Since the latter is the basic signature of the Schwinger vacuum tunneling, the intrinsic gapless 2D graphene layer does not seem to be an ideal candidate for examining QED phenomena.

At this stage another gapped graphene structure is demanded to simulate the electric field induced pp production from vacuum. Armchair graphene nanoribbon (AGNR), a quasi-1D graphene strips with width $d$, surpasses in some sense the graphene layer. In graphene the band gap $\Delta_g$ is the parameter of the theory, associated with the technical parameters (epitaxial growth, elastic strain, Rashba spin splitting on magnetic substrates [36]), modifying the genuine graphene properties, while the AGNR gap $\Delta_r \sim d^{-1}$ [42] is the intrinsic parameter of the untouched graphene. In the case of necessity the band gaps can be measured experimentally, in particular, by optical methods. Since both the AGNR and gapped graphene are semiconductorlike structures, the interband optical absorption spectrum in the vicinity of the threshold $\hbar\omega = \Delta$ demonstrates an easily detected singularity $(\hbar\omega - \Delta_r)^{-1/2}$ and a weakly manifested steplike form $\Theta(\hbar\omega - \Delta_g)$ for the quasi-1D AGNR and 2D graphene layer, respectively. Clearly the first is favorable for the precise band gap measurement. The one-photon absorption of the low intensity light in AGNR has been theoretically studied in a broad range of works [43–48], based on various computational techniques, as well as those related to the graphene layer [5,17,36,38–40]. Undoubtedly, numerical approaches are preferable for an adequate description of concrete experiments. Nevertheless, analytical approaches, being the focus of the present work, are indispensable to elucidate the basic physics of AGNR by deriving closed form analytical expressions for their properties. Our second goal is to promote the application of the AGNR based materials in high-power opto-electronics, using the transparent dependencies of their underlying effects on the ribbon width and strong light wave intensity. However, to the best of our knowledge, in contrast to the graphene layer, explicit results relevant to the dynamically assisted e-h

production and accompanying multiphoton optical absorption in AGNR, irradiated by the intensive light, have virtually not been addressed in the literature yet.

In order to fill this gap we analytically determine the production rate of the e-h pairs, derive the multiphoton interband absorption coefficient and Rabi oscillations frequency in AGNR subject to a time-oscillating electric field of a strong light wave. In addition, we present the pp rate, corresponding to the interband tunneling, caused by the time-constant electric field. We exploit the nearest-neighbors tight-binding model, generating the Dirac equation, to govern the low-energies graphene fermions [1,2] and resonant approximation for particle-wave interaction. The presented results can be employed in two ways. First, properties of the interband multiphoton absorption and e-h tunneling render AGNR a unique material, contributing significantly to applied and fundamental fields of solid state physics. Second, these properties of the graphene ribbon, interpreted as a quantum field theory object, qualitatively highlight the electrically induced instability of a QED vacuum.

The paper is organized as follows. In Sec. II the general approach and basic analytical equations are presented. The Rabi oscillation frequency, rates of the intersubband transitions, associated with the tunneling and multiphoton assisted mechanisms, are derived, discussed, and estimated with respect to future experiments in Sec. III. Section IV contains our conclusions.

## II. GENERAL APPROACH

We consider an electrically biased AGNR, with width $d$ and length $L$, placed on the $x$-$y$ plane and bounded by straight lines $x = \pm d/2$. The time-oscillating electric field $F(t) = F_0 \cos\omega t$, with magnitude $F_0$ and frequency $\omega$, as well as the polarization of the light wave, are chosen to be parallel to the ribbon $y$ axis. The energy spectrum of the free electron in AGNR, derived by Brey and Fertig [42], is a sequence of the 1D subbands with the energies

$$\pm E_N(k) = \left(\varepsilon_N^2 + \hbar^2 v_F^2 k^2\right)^{1/2}, \quad \varepsilon_N = |N - \tilde{\sigma}|\frac{\pi\hbar v_F}{d},$$
$$N = 0, \pm 1, \pm 2, \ldots, \quad \tilde{\sigma} = \frac{Kd}{\pi} - \left[\frac{Kd}{\pi}\right], \tag{3}$$

where $\varepsilon_N$ and $\hbar v_F k$ ($k$ is the wave number) are the size-quantized and continuous energies, corresponding to the transverse ($x$) and longitudinal ($y$) motions, respectively. $v_F = 10^6$ m/s and $K = 4\pi/3a_0$ ($a_0 = 2.46$ Å is the graphene lattice constant) are the Fermi velocity in graphene and the wave number, determining the nonequivalent Dirac points $\vec{K}^{(+,-)} = (\pm K, 0)$ in the graphene Brillouin zone. Below, to be specific, we will consider AGNR of the family $\tilde{\sigma} = 1/3$, providing a semiconductorlike gapped structure.

The general approach to the problem of the optical absorption in AGNR, associated with the interband electron transitions, has been developed in Ref. [49]. For a $y$-polarized light wave, transitions are allowed between the valence and conduction bands, possessing the energies $\mp\,|\,E_N(k)\,|$, respectively. In [49] the dynamical conductivity has been chosen to describe the graphene optical properties. Here, however, we take the traditional for the semiconductorlike structures equivalent characteristic, namely the $l$-photon absorption coefficient $\alpha^{(l)}$, linked to the transition probability $W^{(l)}$ by the following relation:

$$\alpha^{(l)} = \frac{\hbar\omega}{n_b\varepsilon_0 c S F_0^2} W^{(l)}, \quad W^{(l)} = \sum_N W_N^{(l)}. \tag{4}$$

In this equation $n_b$ is the refractive index of the ribbon substrate, $c$ is the speed of light, $S = Ld$ is the area of the ribbon, and $W_N^{(l)}$ is the probability of the transition between the valence and conduction $N$ subbands per unit length per unit time, i.e., the length density of the e-h pair production rate.

The equation, describing the electron at a position $\vec{r}(x, y)$ subject to the external time-dependent electric field, possesses the form of a Dirac equation

$$\hat{H}\vec{\Psi}(\vec{r}, t) = i\hbar\frac{\partial\vec{\Psi}(\vec{r}, t)}{\partial t}, \tag{5}$$

where the Hamiltonian

$$\hat{H}(\vec{k}; y, t) = \hat{H}_x(\hat{k}_x) + \hat{H}_y(\hat{k}_y) + \hat{I}[-eyF(t)], \quad \hat{\vec{k}} = -i\vec{\nabla} \tag{6}$$

is formed by the Hamiltonians

$$\hat{H}_j(\hat{k}_j) = \hbar v_F \begin{pmatrix} -\sigma_j\hat{k}_j & 0 \\ 0 & \sigma_j^*\hat{k}_j \end{pmatrix},$$

relevant to the nonequivalent Dirac points $\vec{K}^{(+,-)}$ [42] and the electric field potential $-eyF(t)$. The matrices $\hat{I}$ and $\vec{\sigma}$ are the unit and Pauli matrices, respectively.

Furthermore, we choose the wave function $\vec{\Psi}$, associated with the $N$ subband, in the form

$$\vec{\Psi}_N(\vec{r}, t) = \frac{1}{\sqrt{2}}[u_{NA}(y, t)\vec{\Phi}_{NA}(x) + u_{NB}(y, t)\vec{\Phi}_{NB}(x)], \tag{7}$$

where $\vec{\Phi}_{NA(B)}$ and $u_{NA(B)}$ are the wave functions describing the electron transverse $x$ and longitudinal $y$ states, governed by the ribbon confinement and electric field $F(t)$, respectively. The indices $A(B)$ mark the graphene sublattices. The explicit form and properties of the four component functions $\vec{\Phi}_{NA(B)}$ are presented in Ref. [50]. The total $x$-wave function

$$\vec{\Phi}_N(x) = \frac{1}{\sqrt{2}}[\vec{\Phi}_{NA}(x) + \vec{\Phi}_{NB}(x)]$$

and the sublattice wave functions $\vec{\Phi}_{NA(B)}$ satisfy the equations

$$\begin{aligned} \hat{H}_x(\hat{k}_x)\vec{\Phi}_{NA(B)} &= \varepsilon_N\vec{\Phi}_{NB(A)}, \\ \hat{H}_x(\hat{k}_x)\vec{\Phi}_N(x) &= \varepsilon_N\vec{\Phi}_N(x), \\ \langle\vec{\Phi}_{N'B(A)}|\vec{\Phi}_{NA(B)}\rangle &= 0\,, \\ \langle\vec{\Phi}_{N'A(B)}|\vec{\Phi}_{NA(B)}\rangle &= \langle\vec{\Phi}_{N'}|\vec{\Phi}_N\rangle = \delta_{N'N}, \end{aligned} \tag{8}$$

where the size-quantized energy levels $\varepsilon_N$ are given in Eq. (3).

Substituting the wave function $\vec{\Psi}_N$ [see Eq. (7)] into Eq. (5) and in view of Eq. (8) we arrive after routine manipulations to a set of equations for the functions $u_{NA(B)}$ with the dropped

indices $N$,

$$\left[\left(-i\hbar\frac{\partial}{\partial t}-eyF(t)\right)\hat{I}+\varepsilon_N\hat{\sigma}_x-i\hbar v_F\frac{\partial}{\partial y}\hat{\sigma}_y\right]\vec{u}=0,$$
$$\vec{u}(y,t)=(u_A(y,t),u_B(y,t)). \quad (9)$$

Solving Eq. (9), the wave function $\vec{\Psi}_N$ in Eq. (7) can be calculated in principle. However, this function does not bring us closer to the solution of the problem of the multiphoton interband transitions. The point is that this problem implies two effects of the electric field $F(t)$, namely the formation of the valence and conduction intraband time-dependent electron states and the generation of the interband transitions between them.

In order to highlight the operators responsible for these effects, we transform Eq. (9) by the substitution

$$\vec{u}(y,t)=\frac{1}{\sqrt{2}}(\hat{\sigma}_z+\hat{\sigma}_x)\hat{U}^+\exp[iq(t)y]\vec{\eta}(t),$$
$$q(t)=\frac{e}{\hbar}\int_0^t F(\tau)d\tau+k,\quad \vec{\eta}(t)=(\eta_1(t),\eta_2(t)), \quad (10)$$

containing the longitudinal momentum $k$. The unitary operator

$$\hat{U}^+=\frac{(\Omega_N+\omega_N)\hat{I}-iv_Fq(t)\hat{\sigma}_x}{[2\Omega_N(\Omega_N+\omega_N)]^{1/2}},$$
$$\Omega_N^2(t)=\omega_N^2+v_F^2q(t)^2,\quad \omega_N=\frac{\varepsilon_N}{\hbar} \quad (11)$$

provides the equation of motion

$$i\hat{I}\dot{\vec{\eta}}=[\Omega_N(t)\hat{\sigma}_z-R_N(t)\hat{\sigma}_x]\vec{\eta},\quad R_N(t)=\frac{\omega_Nv_F\dot{q}(t)}{2\Omega_N^2(t)} \quad (12)$$

for the wave function $\vec{\eta}(t)$. The applied transformation splits the electric field term in Eq. (9) into two components $\sim\Omega_N(t)$ and $\sim R_N(t)$, attributed to the separated valence and conduction intraband states and interband transitions between them, respectively. This transformation is analogous to the Foldy-Wouthuysen one [51], separating completely for $F(t)=0$ the intraband valence and conduction states, corresponding to the energies $\pm E_N(k)$ [Eq. (3)], respectively. In particular, this method has been employed in works dedicated to the interband magnetoelectroabsorption [52] and multiphoton magnetoabsorption [53] in the narrow-gapped bulk semiconductors.

Substituting the function $\eta_{1,2}$ in the form

$$\eta_{1,2}(t)=f_{1,2}(t)\exp\left[\mp i\int_0^t\Omega_N(\tau)d\tau\right]$$

into Eq. (12), we arrive to a set of equations

$$i\dot{f}_{1,2}(t)=-R_N(t)\exp\left[\pm 2i\int_0^t\Omega_N(\tau)d\tau\right]f_{2,1}(t). \quad (13)$$

For the case of a periodically oscillating electric field $F(t)=F_0\cos\omega t$ we select the periodic part in the exponential factor in Eq. (13),

$$\exp\left[2i\int_0^t\Omega_N(\tau)d\tau\right]=\exp\left(\frac{i}{\hbar}\mathscr{E}_Nt\right)S_N(t), \quad (14)$$

where $S_N(t)=S_N(t+\frac{2\pi}{\omega})$ and

$$\mathscr{E}_N=\frac{\hbar\omega}{\pi}\int_{-\frac{\pi}{\omega}}^{+\frac{\pi}{\omega}}\Omega_N(t)dt. \quad (15)$$

Since the term $\hbar^2\Omega_N^2(t)$ is the eigenvalue of the intraband Hamiltonian $[-\hbar v_Fq(t)\hat{\sigma}_y+\varepsilon_N\hat{\sigma}_z]^2$, the quasienergy $\mathscr{E}_N$ (15) can be treated as the change of the electron quasienergy, caused by the transition between the valence and conduction $N$ subbands or, equivalently, the quasienergy of the created e-h pair. In addition, it is reasonable to exploit in Eqs. (13) the expansion of the time-periodic product $R_N(t)S_N(t)$ in the Fourier series

$$R_N(t)S_N(t)=\sum_{l=-\infty}^{+\infty}A_le^{-il\omega t}, \quad (16)$$

where

$$A_l(\omega)=\frac{\omega}{2\pi}\int_{-\frac{\pi}{\omega}}^{+\frac{\pi}{\omega}}R_N(t)S_N(t)e^{il\omega t}dt. \quad (17)$$

Since the exact equations (13) do not admit an analytical solution, we consider this set in the resonant approximation $\omega_l\ll\omega(\omega_l=\mathscr{E}_N/\hbar-l\omega)$, implying the significant proximity of the e-h pair quasienergy $\mathscr{E}_N$ to the total energy $l\hbar\omega$ of $l$ involved photons. Averaging the coefficients in Eqs. (13) in view of Eqs. (14), (15), and (16), we obtain the following relations:

$$i\dot{\bar{f}}_1=-\bar{f}_2A_le^{i\omega_lt},\quad i\dot{\bar{f}}_2=-\bar{f}_1A_l^*e^{-i\omega_lt}, \quad (18)$$

where $\bar{f}_{1,2}(t)$ are the functions $f_{1,2}(t)$ averaged over the electric field period $T=2\pi/\omega$ in the vicinity of the time instant $t$,

$$\bar{f}_{1,2}(t)=\frac{1}{T}\int_{t-\frac{T}{2}}^{t+\frac{T}{2}}f_{1,2}(\tau)d\tau.$$

Equations (18) describe the well known two-level problem [54]. Under the initial conditions $\bar{f}_1(0)=0$, $\bar{f}_2(0)=1$ the solution to Eqs. (18) becomes

$$\bar{f}_1(t)=iA_l\frac{\sin\lambda_lt}{\lambda_l}e^{\frac{i}{2}\omega_lt},$$
$$\bar{f}_2(t)=\left(\cos\lambda_lt+\frac{i\omega_l}{2\lambda_l}\sin\lambda_lt\right)e^{-\frac{i}{2}\omega_lt}, \quad (19)$$
$$\lambda_l=\left(|A_l|^2+\frac{1}{4}\omega_l^2\right)^{1/2},\quad l=1,2,\ldots,$$

where the quasienergy $\mathscr{E}_N$ and coefficients $A_l$ are given by Eqs. (15) and (17), respectively. The derived equations are valid under the condition $\lambda_l\ll\omega$, i.e., the resonant approximation.

From the above procedure of determining the functions $\bar{f}_{1,2}(t)$ [Eq. (19)] and their meanings, the differential probability $w_N^{(l)}(k)$ of the interband electron transition between the valence and conduction $N$th subbands can be written in the form $w_N^{(l)}(k)=|\bar{f}_1(t)|^2$, to give in view of Eq. (19)

$$w_N^{(l)}(k)=|A_l(k)|^2\frac{\sin^2\lambda_lt}{\lambda_l^2}. \quad (20)$$

In an effort to continue the analytical investigations, the explicit form of the coefficient $A_l$ is needed. In view of Eqs. (12) and (14) for the functions $R_N(t)$ and $S_N(t)$, respectively, and under the condition $\mathscr{E}_N = l\hbar\omega$ the coefficient $A_l(k)$ in Eq. (17) acquires the closed integral form

$$\frac{2\gamma_N}{\omega}A_l(k) = \frac{1}{2\pi}\int_{-\pi}^{+\pi}\frac{\exp\left[il\int_0^{\varphi}\Lambda^{1/2}(\psi,u)d\psi\right]}{\Lambda(\varphi,u)}\cos\varphi d\varphi,$$
$$\Lambda(\varphi,u) = 1+\gamma_N^{-2}(\sin\varphi+u)^2, \qquad (21)$$
$$u = \frac{\hbar\omega k}{eF_0}, \quad \gamma_N = \frac{\omega\Delta_N}{2ev_FF_0},$$

while the quasienergy $\mathscr{E}_N$ is obtained explicitly:

$$\mathscr{E}_N(k) = \frac{2}{\pi}\Delta_N\frac{1}{s_N}E\left(\sqrt{1-s_N^2}\right)\left(1+s_N^2\frac{2\hbar^2v_F^2k^2}{\Delta_N^2}\right),$$
$$s_N^2 = \left(1+\gamma_N^{-2}\right)^{-1}. \qquad (22)$$

In Eqs. (21) and (22) $\Delta_N = 2\varepsilon_N$ is the intersubband energy gap, $E(x)$ is the complete elliptic integral of the second kind [55], and $\gamma_N$ is the Keldysh adiabaticity parameter [18], determining the intersubband transition mechanism. For $\gamma_N \ll 1$ the e-h pp is generated by the Zener tunneling in an approximately constant electric field $F_0$, while for $\gamma_N \gg 1$ the multiphoton assisted mechanism dominates.

The employed further condition $l \gg 1$ allows us to perform analytically the integration in Eq. (21) by the steepest-descent method, treating the number of absorbed photons $l$ as a large parameter. Note that the below-determined total probability includes the term $\sim|A_l(k)|^2g(k)\frac{dk}{d\mathscr{E}_N}$, where for the quasi-1D AGNR the density of $k$ states $g(k) = \text{const.}$ and $\frac{dk}{d\mathscr{E}_N} \sim k^{-1}$ [see Eq. (22)]. Thus, the term $|A_l(0)|$ is sufficient for the description of the optical transition in the vicinity of the spectral singularity $k = 0$.

Since the differential probability $\sim|A_l(k)|^2$ [Eq. (20)] and the corresponding Rabi oscillation frequencies $\sim|A_l(k)|$ reach a maximum for $k = 0$ both in graphene [36], and in the AGNR [see Eq. (21)], we further focus on the coefficient $|A_l(0)|$. Though analogous integrals have appeared earlier in Refs. [18,56,57], a brief outlook onto the needed techniques seems to be in place here. The integration segment $(-\pi,0) \to +(\pi,0)$ in Eq. (21) is replaced by a contour, consisting of additional segments $(\pi,0) \to (\pi,-\infty) \to (-\pi,-\infty) \to (-\pi,0)$. Note that the saddle points $\varphi_n = \arcsin(i\gamma_N + n\pi); n = 0,\pm1$, at which the function $\Lambda(\varphi,0)$ vanishes, coincide with the poles of the integrand. In this case the steepest-descent method implies the subsequent bypassing of the saddle points $\varphi_1, \varphi_0, \varphi_{-1}$, positioned inside the corresponding three segments. The bypassing arcs with the vanishing small radius are $2\pi/3$ and $4\pi/3$ for the saddle points $\varphi_{\pm1}$ and $\varphi_0$, respectively. In view of the saddle points total contribution, the calculation reduces to the contour integration around the pole $\varphi_0$. The residue theorem gives then

$$A_l(0) = \frac{\omega}{3}\exp\left\{-\frac{l}{s_N}[K(s_N)-E(s_N)]\right\}\sin^2\frac{l\pi}{2}, \qquad (23)$$

where $K(x)$ is the complete elliptic integral of the first kind [55]. The factor $\sin^2\frac{l\pi}{2}$ stems from the interference of the saddle points and the condition $l\hbar\omega = \mathscr{E}_N$ (see Ref. [58] for more details).

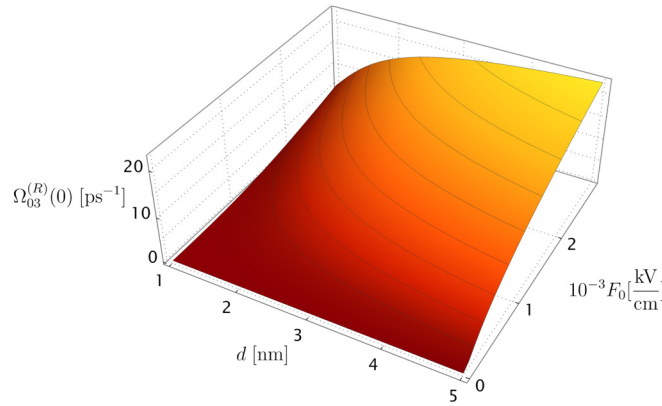


FIG. 1. The Rabi frequency $\Omega_{03}^{(R)}(0)$ versus the ribbon width $d$ and electric field $F_0$. The frequency $\Omega_{0l}^{(R)}(0)$ is determined by Eqs. (23) and (24), describing the three-photon $l = 3$ oscillations between the ground subbands $N = 0$.

## III. RESULTS AND DISCUSSION

### A. Rabi oscillations

Equation (20) describes periodic oscillations with the Rabi frequency $\Omega_{Nl}^{(R)} = 2\lambda_l$. Under the condition $\omega_l/2 \ll |A_l|$ the transition probability $w_N^{(l)} = \sin^2|A_l|t$ oscillates with the Rabi frequency

$$\Omega_{Nl}^{(R)}(k) = 2|A_l(k)|. \qquad (24)$$

For the cases of the tunneling $\gamma_N \ll 1$, $\Omega_{Nl}^{(R)} \equiv \Omega_{N\text{tun}}^{(R)}$ and the multiphoton $\gamma_N \gg 1$ regimes the Rabi frequency, determined from Eqs. (23) and (24) for the zero longitudinal momentum $k$, reads

$$\Omega_N^{(R)}(0) = \frac{2}{3}\omega\begin{cases}\frac{1}{3}\exp\left(-\frac{\pi F_c^{(N)}}{2F_0}\right), & \gamma_N \ll 1,\\ \exp(l)(4\gamma_N)^{-l}\sin^2\frac{l\pi}{2}, & \gamma_N \gg 1,\end{cases}$$
$$F_c^{(N)} = \frac{\Delta_N^2}{4\hbar v_Fe}, \qquad (25)$$

where $F_c^{(N)}$ is the breakdown electric field, delimiting the active and suppressed tunneling for the fields $F_0 > F_c^{(N)}$ and $F_0 < F_c^{(N)}$, respectively. In the presence of the critical field, the electron in the AGNR with the effective mass $m = \Delta_N/2v_F^2$ acquires for the Compton wavelength an energy comparable to the energy gap $\Delta_N$. Equations (23), (24), and (25) allow us to trace the dependencies of the Rabi frequency on the electric field and ribbon width in the vicinity of the resonance $\omega_l \simeq 0$. The photon assisted transitions are allowed only for the odd numbers $l = 1,3,5,\ldots$. With increasing electric field $F_0$, driving frequency $\omega = \frac{\mathscr{E}_N}{\hbar l}$, and ribbon width $d$, the Rabi frequency $\Omega_{Nl}^{(R)}(0)$ increases for any regime. The Rabi frequency $\Omega_{Nl}^{(R)}(0)$ according to Eqs. (23) and (24) as a function of the ribbon width and electric field, is depicted in Fig. 1. Figure 2 shows the isofrequency lines $\Omega_N^{(R)}(0;F_0,d) = \text{const}$.

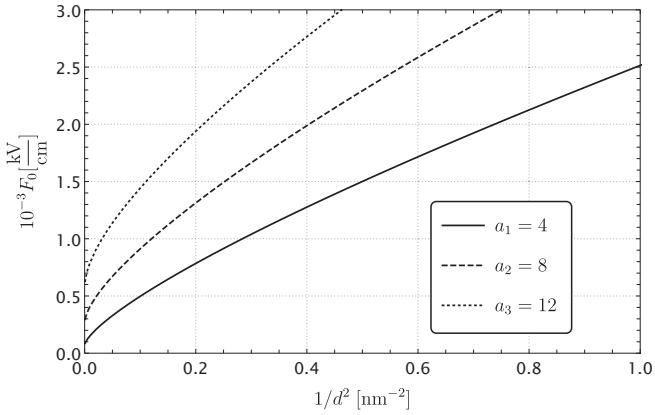


FIG. 2. The isofrequency curves $\Omega_{03}^{(R)}(0; d, F_0) = a_j$, $j = 1, 2, 3$, linking the ribbon width $d$ and electric field $F_0$. Equations (23) and (24) for the ground $N = 0$ three-photon $l = 3$ transitions are employed.

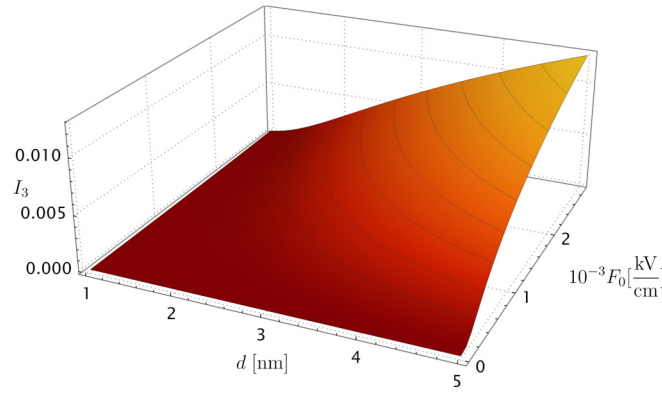


FIG. 3. The dependence of the dimensionless peak intensity $I_3$ on the ribbon width $d$ and electric field $F_0$. It is obtained from Eq. (28) for $I_3$, adapted to the three-photon $l = 3$ absorption, induced by the transitions between the ground $N = 0$ subbands.

### B. Intersubband transitions

#### 1. Multiphoton assisted transitions

If the detuning $\omega_l$ dominates in Eqs. (19) and (20), then, in view of the general results of time-dependent perturbation theory [54], the total probability of the $l$-photon intersubband transition per unit length per unit time acquires the form

$$W_N^{(l)} = \frac{1}{2\pi}\int dk 2\pi\hbar |A_l(k)|^2 \delta[\mathscr{E}_N(k) - l\hbar\omega], \tag{26}$$

where the $\delta$ function reflects the energy conservation in the system of the e-h pair and absorbed $l$ photons. Substituting the coefficient $A_l$ and energy $\mathscr{E}_N$ from Eqs. (23) and (22), respectively, we obtain for the length density of the e-h pp rate

$$W_N^{(l)} = \frac{\pi^{1/2}}{36}\frac{\omega^2}{v_F} I_l(s_N) G_l^{-1/2}(\omega) \sin^4\frac{l\pi}{2}, \tag{27}$$

which in turn determines the $l$-photon absorption coefficient $\alpha^{(l)}$ in Eq. (4). In Eq. (27) the functions

$$I_l(s_N) = s_N^{-1/2} E^{-1/2}\left(\sqrt{1 - s_N^2}\right) \times \exp\left\{-\frac{2l}{s_N}[K(s_N) - E(s_N)]\right\} \tag{28}$$

and

$$G_l(\omega) = \frac{l\hbar\omega}{\Delta_N} - \frac{2}{\pi s_N} E\left(\sqrt{1 - s_N^2}\right) \tag{29}$$

are responsible for the spectral intensity and position of the absorption singularity $\sim G_l^{-1/2}$, respectively.

For the limiting case $\gamma_N \gg 1$ the functions $I_l(s_N)$ and $G_l(\omega)$ become

$$I_l(\gamma_N) = \left(\frac{2}{\pi}\right)^{1/2} \exp(2l)\left(\frac{1}{16\gamma_N^2}\right)^l \tag{30}$$

and

$$G_l(\omega) = \frac{l\hbar\omega}{\Delta_N} - \left(1 + \frac{1}{4\gamma_N^2}\right), \tag{31}$$

respectively.

Equations (27), (30), and (31) explicitly demonstrate the dependencies of the multiphoton intersubband absorption spectrum (4) on the parity of the absorbed photon number $l$, subband number $N$, ribbon width $d$, and electric field $F_0$. As a result of the saddle points $\varphi_{0,\pm1}$ interference in the integrand of Eq. (21) the spectral singularities $\sim G_l^{-1/2}$ in $W_N^{(l)}$ (27) are allowed only for the odd numbers $l = 1, 3, \ldots$. The greater the photon number $l$ is, the less the corresponding intensity $I_l$ in Eq. (30). With increasing subband number $N$ the peak positions, determined by the condition $G_l(\omega) = 0$ in Eq. (31), shift towards high frequencies and decrease in intensity. As the ribbon becomes narrower, the peaks move to the high frequency region $l\hbar\omega \sim d^{-1}$ and reduce in magnitude $\sim d^{2l}$. The larger the electric field $F_0$ is, the larger are both the shift of the peak position to higher frequencies $\sim F_0^2$, and its maximum $I_l \sim F_0^{2l}$. For the general case for an arbitrary $\gamma_N$ the dependency of the peak intensity $I_l$ [Eq. (28)] on the electric field $F_0$ and ribbon width $d$ are shown in Fig. 3. Figure 4 demonstrates the isointensity curves $I_l(F_0, d) = \text{const}$.

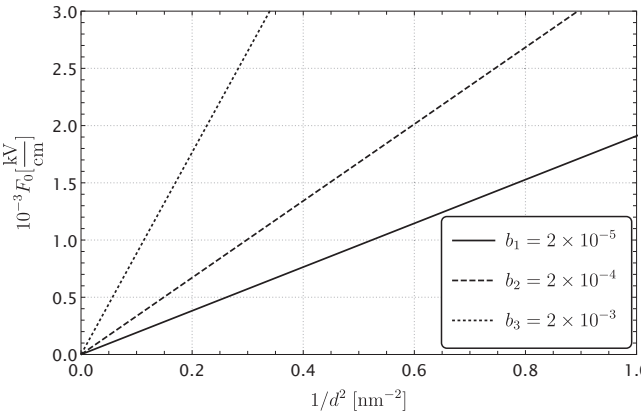


FIG. 4. The isointensity curves $I_3(d, F_0) = b_j$, $j = 1, 2, 3$, related to the ribbon width $d$ and electric field $F_0$. Equation (28) for $I_3$ is employed for the three-photon $l = 3$ transitions between the ground $N = 0$ subbands.

### 2. Tunneling

In the case of small frequencies $\omega$ and considerable electric fields $F_0$, i.e., $\gamma_N \ll 1$ ($\omega \to 0$) the transitions happen due to the intersubband tunneling in a practically stationary electric field $F_0$. Based on the calculation of the probability $W_N = \sum_l W_N^{(l)}$ by means of $\sum_l$ by $\int \frac{1}{\omega} d(l\omega)$ and Eq. (27) by $W_N^{(l)}$, correctly reproduces the exponential behavior

$$W_N \sim \exp\left(-\frac{\pi F_c^{(N)}}{F_0}\right),$$

coinciding with those obtained earlier in Refs. [18,56]. The dimensionless prefactor $\hbar v_F e F_0/\Delta_N^2$ appears to be incorrect. As pointed out in Ref. [18], this stems from the fact that the limiting transition $\omega \to 0$ applies to the results based on the averaging over the finite period $T = 2\pi/\omega$ of the oscillating electric field. The corresponding correct analysis of the intersubband tunneling should however treat the electric field to be adiabatically slow from the beginning.

The proper determination of the differential probability $w_N(\vec{k})$ started in the 1950s on account of the vacuum decay in the presence of a constant electric field [9]. This study was continued in the 1970s further. The various approaches, namely the imaginary time method [59], parabolic cylinder functions [10,13,15,26,28,60], Ricccati [15,61] and quantum kinetic equations (QKE) were proposed [16,62–64]. Notice that the probability $W_N$ can be calculated within the present approach. Indeed, it was shown that the set of initial Eqs. (9) is trivially reduced to the oscillatorlike equations for the parabolic cylinder functions [26,28], while the set (13) for the functions $f_{1,2}(k,t)$ is equivalent to the Riccati [15,61] and/or (QKE) [62–64] equations for the functions $|f_1(k,t)|$ and $|f_1(k,t)|^2$, respectively. The details of the transformation of Eqs. (13) into the QKE are given, in particular, in Ref. [64]. In addition, Fedotov *et al.* [16], based on the exact solution to QKE, have calculated the differential distribution function for the interband transition probability, i.e., the mean number of pairs $w_N(\vec{k})$ created in a given quantum state, completely coinciding with those derived by others of the above-listed methods. The underlying analysis is transparently presented in Refs. [16,64] and we provide here for reasons of brevity only their results in an explicit form

$$w_N(\vec{k}) = 2\exp\left[-\frac{\pi\left(\varepsilon_N^2 + \hbar^2 v_F^2 \vec{k}_\perp^2\right)}{\hbar v_F e F_0}\right],$$
$$W_N^{(n)} = \frac{1}{(2\pi)^n T}\int w_N(\vec{k}) d^n\vec{k}, \tag{32}$$

where $W_N^{(n)}$ is the spatial density of the tunneling probability rate [6] in the $n$-dimensional structure. In Eq. (33) the prefactor two takes into account the spin projections, $\vec{k}[\vec{k}_\perp, k]$ is the wave vector, and $\varepsilon_N$ is the energy gap. Integration in Eq. (32) over $k$ implies $\int dk = eF_0T/\hbar$ [26], where $T$ is the total (infinitely large) lifetime of the DC electric field (see Refs. [13,28] for details).

For the quasi-1D AGNR ($n = 1$) Eq. (32), in view of the two valleys ($K^{\pm}$) [26,36,39], generates the mean total number of the e-h pairs per unit length per unit time, created due to the tunneling transition via the subband gap $\Delta_N = 2\varepsilon_N$ [Eq. (3)],

$$W_N^{(1)} \equiv W_{N\text{tun}} = \frac{2eF_0}{\pi\hbar}\exp\left[-\frac{\pi F_c^{(N)}}{F_0}\right]. \tag{33}$$

The same result, accurate to the spin and valley factors, has been derived by Gavrilov and Gitman [28] for the 1D spatial states in the framework of an exact solution to the Dirac equation. In addition, just the same approach has been employed to study the mathematically exactly solvable problem of particle production from a QED vacuum by the Sauter-like and peak time depending electric field [65]. The total length density of the e-h pp rate $W_N = \sum_N W_{N\text{tun}}$ is derived from Eq. (33). In the limiting case $d \to \infty$ the latter equation with the replacement $\sum_N$ by $d\int d(\frac{N}{d})$ results, as expected, in the square density rate for the gapless ($d^{-1} \sim \Delta_N \to 0$) graphene layer

$$W_g = \frac{1}{\pi^2 v_F^{1/2}}\left(\frac{eF_0}{\hbar}\right)^{3/2},$$

presented, in particular, in Refs. [26,36].

A doubled rate $2W_v$ of the electron-positron pair production from the "1D vacuum" can be obtained from Eq. (33) by replacing $v_F$ by $c$ and $\Delta_N$ by $2mc^2$. Equation (32) has been used by other authors; for the 3D and 2D spaces Eq. (32) reproduces the vacuum ($\varepsilon = mc^2$, $v_F = c$) [6,9,13] and gapless ($\varepsilon = 0$) [26] graphene rates, respectively. The rate (33) differs from the one calculated in Ref. [64] by a factor of 4, because of the spin and valley factors which both equal 2. Note that Eq. (32), describing the time-independent effect, can be obtained by the WKB method, while for the multiphoton assisted processes [see Eq. (30)] the semiclassical approximation is inappropriate [31].

Clearly the length density of the e-h pp tunneling rate $W_{N\text{tun}}$ [Eq. (33)] increases with both increasing the electric field $F_0$ and ribbon width $d$ according to Fig. 5. The isorate diagrams $W_{0\text{tun}}(F_0, d) = \text{const.}$ are depicted in Fig. 6. It is appropriate here to point out the common property of the isovalue diagrams. Figures 2 and 6 demonstrate the practically linear relationship with respect to the considerable electric fields $F_0$ and the square of the reciprocal width $1/d^2$ of the narrow ribbons. As expected, deviations from the linear law occur for weak electric fields and wide ribbons. The reason for this is that the latter closely resemble more of the graphene layer

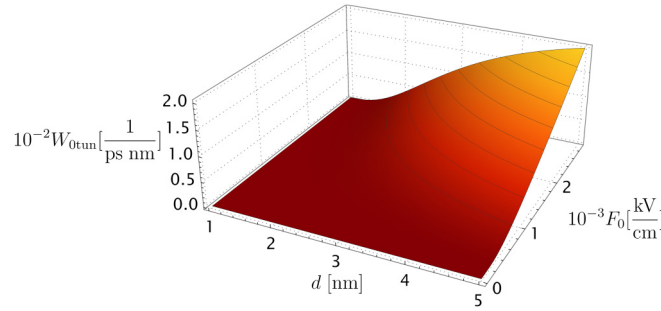


FIG. 5. The length density of the pair production rate $W_{0\text{tun}}$ [Eq. (33)], caused by the electron tunneling between the ground $N = 0$ subbands in the ribbon with width $d$ in the presence of an electric field $F_0$.

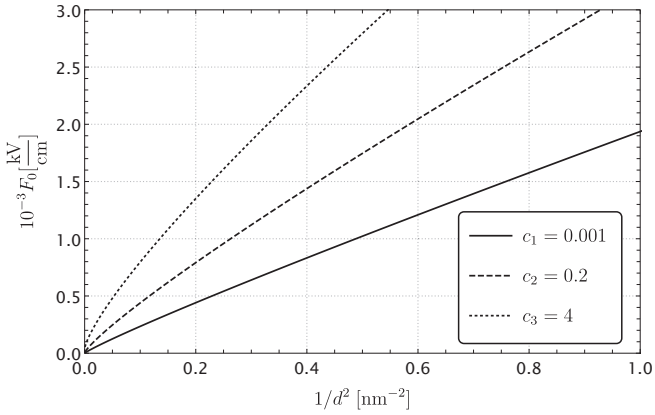


FIG. 6. The isorate diagrams $W_{0\text{tun}}(d, F_0)$ (nm ps)$^{-1} = c_j$, $j = 1, 2, 3$. calculated from Eq. (33) for the tunneling between the ground $N = 0$ subbands.

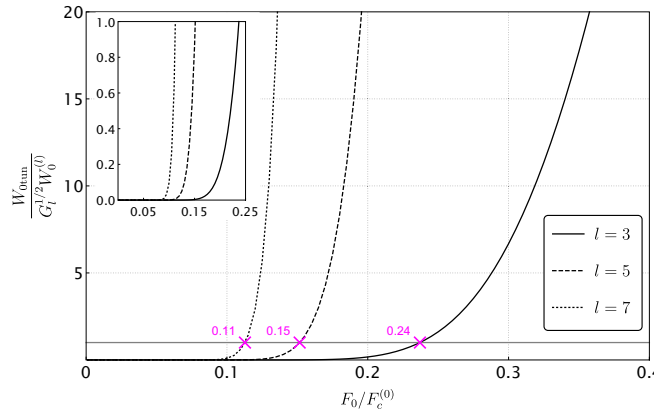


FIG. 8. The ratio of the tunneling $W_{0\text{tun}}$ (33) and photon assisted $G_l^{1/2}W_0^{(l)}$ [Eq. (27)] length density rates as a function of the dimensionless electric field $F_0/F_c^{(0)}$ for the $l$-photon ($l = 3, 5, 7$) transitions between the ground $N = 0$ subbands for which $F_c^{(0)} = 2.0 \times 10^3$ kV/cm.

than a ribbon. Figure 4 shows the strict linear dependence $F_0 \sim 1/d^2$. Note here that the correct description of the wide ribbon and the graphene layer implies the summation over the subband index $N$ of the rates $w_N^{(l)}(k)$ [Eqs. (20) and (24)], $W_N^{(l)}$ [Eq. (27)], and $W_{N\text{tun}}$ [Eq. (33)] for the Rabi oscillations, multiphoton assisted, and tunneling transitions, respectively.

Using the relation between the differential probability $w_N(\vec{k})$ [Eq. (32)] and an AGNR to an AGNR $N$ transition probability $\mathscr{P}_N$ [28,65], i.e., the probability for an AGNR to electronically remain an AGNR on account of the tunneling between the $N$ subbands

$$\mathscr{P}_N = \exp\left\{\int d\vec{k}\ln[1 - 2w_N(\vec{k})]\right\}$$

and integrating over the momentum $k$ by the same method, taken in Eq. (32) we obtain

$$\frac{\ln \mathscr{P}_N}{LT} = \frac{2eF_0}{\pi\hbar}\ln\left[1 - \exp\left(-\frac{\pi F_c^{(N)}}{F_0}\right)\right]. \qquad (34)$$

The greater the electric field and the wider the ribbon are, the less is the ribbon stability $\mathscr{P}_N$. The dependence of the probability $\mathscr{P}_0$ w.r.t. the ground transition $N = 0$ on the electric field $F_0$ and width $d$ is shown in Fig. 7.

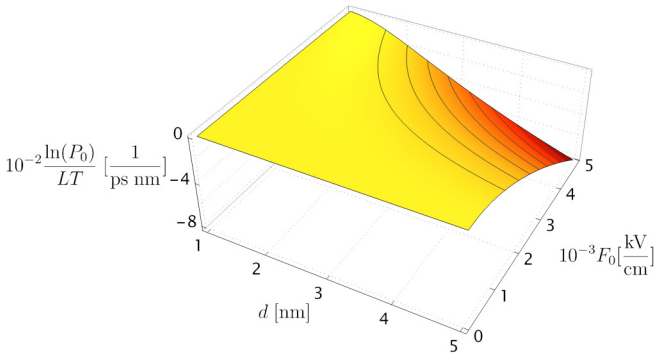


FIG. 7. The logarithm of the length density rate of the probability $\mathscr{P}_0$ as a function of the electric field $F_0$ and ribbon width $d$, calculated from Eq. (34) for the ground transition $N = 0$. $T$ and $L$ are the radiation exposition time and ribbon width $d$, respectively.

In order to highlight the contribution of the time dependence of the electric field to the e-h pair production, we investigate the dependence of the ratio of the tunneling $W_{0\text{tun}}$ [Eq. (33)] and photon assisted $G_l^{1/2}W_0^{(l)}$ [Eq. (27)] rates on the electric field $F_0$. Figure 8 shows this ratio as a function of the electric field $F_0$. These graphs, based on Eqs. (27) and (33), demonstrate that in the region of weak electric fields $F_0/F_c^{(0)} \ll 1$ the photon assisted rate surpasses that of tunneling. With the electric field approaching the values $F_0/F_c^{(0)} \simeq 1$ the advantage of the photon assisted mechanism reduces, and both rates become comparable and further, for $F_0 \geqslant F_c^{(0)}$, the tunneling process dominates that of photonic absorption.

The reason for the above described evolution is that the electric field change generates a change of the transition regime. For weak electric fields $F_0 \ll F_c^{(0)}$ and low frequencies $\omega < \Delta_0/\hbar$ the intersubband tunneling time $\tau_0 = \Delta_0/eF_0v_F$ exceeds the half-cycle $T/2 = \pi/\omega$ ($\tau_0 > T/2$, $\gamma_0 \gg 1$), and the fast oscillating ($\omega > \tau_0^{-1}$) field prevents the tunneling and promotes the involvement of the $l \simeq \Delta_0/\hbar\omega$ photons in the intersubband transitions. With the growth of the electric field towards values exceeding the critical one $F_0 \geqslant F_c^{(0)}$, the opposite conditions $\tau_0 < T/2$, $\gamma_0 \geqslant 1$ allow us to treat the intersubband transitions as a tunneling process induced by the nearly constant ($\omega < \tau_0^{-1}$) electric field $F(t) = F_0$. The role of the time dependence of a relatively weak $F_0 < F_c^{(0)}$ electric field for the enhancement of the pp rate, revealed here for the AGNR, is absolutely analogous to that for the electrically biased graphene layer, studied numerically in Ref. [36] (see also [38,39] for details). However, we refrain from a detailed quantitative comparison of our results to those presented for the graphene layer. The reason for this is that the prefactor in Eq. (33) $\sim F_0$ and the states energy density factor in Eq. (27) $\sim G_l^{-1/2}$ differ from the corresponding ones for the 2D structures, namely $\sim F_0^{3/2}$ [36] and $\sim$const., respectively. Clearly accounting for the electron interaction with the phonons and impurities, manifesting itself in replacing the root singularity in Eq. (27) by a finite value, would lead to a more adequate description of the electronic

TABLE I. The dimensionless threshold $p^{(l)}_{0\text{thr}} = F^{(l)}_{0\text{thr}}/F^{(0)}_c$ and balanced $p^{(l)}_{0b} = F^{(l)}_{0b}/F^{(0)}_c$ electric fields, delimiting the $l$-photon assisted and tunneling regimes ($\gamma^{(l)}_N = 1$) and providing the balance between its rates ($W_{0^{(l)}} = W_{0\text{tun}}$), respectively. Fields scaled to the critical electric field $F^{(0)}_c$.

| l | $p^{(l)}_{0\text{thr}}$ | $p^{(l)}_{0b}$ | $p^{(l)}_{0\text{thr}}/p^{(l)}_{0b}$ |
|---|---|---|---|
| 3 | 0.74 | 0.24 | 3.0 |
| 5 | 0.45 | 0.15 | 3.0 |
| 7 | 0.32 | 0.11 | 2.9 |

and optical effects in AGNR. However, this problem is a subject for further possible consideration.

Figure 8 allows us to reveal the relationship between the key electric fields, characterizing the given $N$ intersubband transition. First one is the threshold field $F^{(l)}_{0\text{thr}}$, determined by the critical resonant Keldysh parameter $\gamma^{(l)}_N = 1$, in which [see Eq. (21)] the frequency $\omega$ satisfies the resonant condition $\mathscr{E}_N(0) = l\hbar\omega$, where $\mathscr{E}_N(0)$ is determined from Eq. (22). The field $F^{(l)}_{0\text{thr}}$ qualitatively delimits the tunneling ($F_0 < F^{(l)}_{0\text{thr}}, \gamma^{(l)}_N < 1$) and $l$-photon assisted ($F_0 > F^{(l)}_{0\text{thr}}, \gamma^{(l)}_N > 1$) type transitions. On account of the elliptic integral of the second kind, $E[(1+\gamma^2_N)^{-1/2}]$ it changes smoothly in the vicinity of $\gamma_N \simeq 1$. and we set $E(2^{-1/2}) = 1.23$ to obtain the resonant Keldysh parameter $\gamma^{(l)}_N$ [Eq. (21)],

$$\gamma^{(l)2}_N = \frac{1}{2} + \sqrt{\frac{a^2}{4} + a}; a = \left(\frac{\pi}{2lp_N}\right)^2, \quad p_N = \frac{F_0}{F^{(N)}_c}.$$

This equation links the resonant Keldysh parameter $\gamma^{(l)}_N$ with the electric field $F_0$ and number of photons $l$ in the intermediate region $\gamma^{(l)}_N \simeq 1$. For $\gamma^{(l)}_N = 1$ the exact value of the threshold dimensionless electric field, calculated from the resonant condition, reads

$$p^{(l)}_{N\text{thr}} = \frac{\pi}{\sqrt{2}l}.$$

The second key, so-called balanced electric field $F^{(l)}_{0_b}$, equalizes the tunneling and $l$-photon assisted rates. Calculating the threshold $p^{(l)}_{N\text{thr}} = \frac{\pi}{\sqrt{2}l}$ and balanced $p^{(l)}_{N_b}$ dimensionless electric fields for the ground transition $N = 0$ from the given above equation and from Fig. 8, respectively, we present the result of their comparison in Table I.

The ratio of the electric fields under discussion, being $p^{(l)}_{0\text{thr}}/p^{(l)}_{0b} = 3$, does not depend on the number of photons $l$. Thus, experimentally measuring the ratio of the rates $W^{(l)}_N$ and $W_{N\text{tun}}$ as a function of the electric field, we find the balance field $p^{(l)}_{Nb}$ and in the case of known $p^{(l_0)}_{N\text{thr}}$ for the specific $l_0$, physically important dimensionless electric fields for other values of $l$ can be found.

The effect of the oscillating character of the electric field on the Rabi oscillations is qualitatively the same as that on the above discussed intersubband transitions. For weak electric fields $F_0 \ll F^{(N)}_c$ their time periodic resonant oscillations significantly increase the multiphoton assisted Rabi frequencies $\Omega^{(R)}_{Nl}$, making them much greater than the corresponding $\Omega^{(R)}_{N\text{tun}}$, induced by the tunneling for approximately constant electric field. With increasing electric field strength towards the values $F_0 \simeq F^{(N)}_c$ these Rabi frequencies align ($\Omega^{(R)}_{Nl} \simeq \Omega^{(R)}_{N\text{tun}}$), then the electric field time dependence becomes ineffective ($\Omega^{(R)}_{Nl} < \Omega^{(R)}_{N\text{tun}}$). The electric fields, providing the Rabi frequency balance ($\Omega^{(R)}_{Nl} = \Omega^{(R)}_{N\text{tun}}$), decrease with an increasing number of involved photons $l$. The dependence of the ratio $\Omega^{(R)}_{N\text{tun}}/\Omega^{(R)}_{Nl}$ on the dimensionless electric field $F_0/F^{(N)}_c$ closely resembles that presented in Fig. 8.

All aforementioned conclusions in this section, related to the ground $N = 0$ e-h subband, apply qualitatively also for excited ones with $N \neq 0$. It is reasonable to note here that, similar to works [6,17,36,60,64], our approach ignored the collisions between the created pairs and backreaction of their inherent electric field to the applied external one. However, these effects might be expected to be insignificant due to the relatively small density of the created e-h pairs, that in turn depends not only on the electric field magnitude $F_0$, but on the exposure time $T$. In any case these phenomena require special consideration, in particular, in the framework of a quantum kinetic equation [16].

### C. Estimates of the expected experimental values

Focusing on possible experiments, we estimate the expected values for the gapped AGNR for a width of 2 nm exposed to a light wave of $\omega = 330\ \text{ps}^{-1}$($\lambda = 5.4\ \mu\text{m}$) and electric field $F_0 = 500\ \text{kV/cm}$. This corresponds to a light intensity $I = 6.5 \times 10^5\ \text{kW/cm}^2$ and obeys the resonant condition $G_l = 0$ [Eq. (29)] for the number of photons $l = 3$ and ground ($N = 0$) energy gap $\Delta_0 = 2\varepsilon_0 = 0.69\ \text{eV}$ [Eq. (3)]. The multiphoton and tunneling rates $W^{(3)}_0 G^{1/2}_3$ and $W_{0\text{tun}}$, calculated from Eqs. (27) and (33), respectively, become $0.86 \times 10^{-4}$ and $1.4 \times 10^{-4}$ 1/nm ps, respectively. For the electric field $F_0 = 470\ \text{kV/cm}$ they reach a balance equal to $1.4 \times 10^{-3}$ $1/nm$ ps and with increasing the electric field the tunneling mechanism dominates that of multiphoton transitions. The "to remain" probability $\mathscr{P}_N$, calculated from Eq. (34) for the ground $N = 0$ subbands and electric fields $F_0 = F^{(0)}_c = 2.0 \times 10^3\ \text{kV/cm}$, reads $(LT)^{-1} \ln \mathscr{P}_0 = -8.48$ $1/nm$ ps.

The chosen ribbon ($d$) and electric field ($F_0, \omega$) characteristics result in $\Omega^{(R)}_{03}(0) \simeq 1.21\ \text{ps}^{-1}$ [Eqs. (23) and (24)] for the Rabi frequency and $\Omega^{(R)}_{03}(0)/\omega \simeq 3.7 \times 10^{-3} \ll 1$ for the frequencies ratio. Note that the vacuum related breakdown electric field $F^{(v)}_c$ exceeds its counterpart $F^{(0)}_c = 2.0 \times 10^3\ \text{kV/cm}$ for the ground gap $\Delta_0$ by a factor of $10^{10}$.

We believe that the analytical approach developed here contributes to gaining insights into the physics of the intersubband transition in AGNR and QED vacuum decay, both media being subject to a strong light wave. Also, we hope the estimates of the expected experimental values could be useful for further studies of graphene nanoribbons and their applications in opto- and microelectronics as well as the vacuum phenomena.

## IV. SUMMARY AND CONCLUSION

We have developed an analytical approach to the problem of the Rabi oscillations and intersubband absorption of a strong light wave in an armchair graphene nanorib-

bon (AGNR). Based on the Dirac equation, describing the massless electron in the vicinity of the Dirac points, we have derived analytical expressions for the length density of the electron-hole differential pair production (pp) rate. The resonant approximation, implying a balance between the photons energies and intersubband quasienergetic gaps, has been employed. This rate in turn determines explicitly the Rabi oscillation frequency and absorption coefficient for tunneling and multiphoton assisted intersubband transition regimes. The obtained results allow us to trace the explicit dependencies of the Rabi frequency and pp rate on the ribbon width, electric field strength, and parity of the involved photons. The odd-photon absorption spectra demonstrate the reciprocal square root singularities in the vicinity of the resonant frequencies. With increasing the electric field and widening the ribbon both the Rabi frequency and pp rate increase. For relatively weak electric fields the oscillating character of the electric field enhances the intersubband transitions and multiphoton assisted effects contribute significantly stronger than the tunneling ones. With further increase of the electric field these effects become equal and finally the tunneling mechanism surpasses that of multiphoton processes. The latter dependence completely correlates with the previously numerically calculated one for the gapped graphene layer. Estimates of the expected values show that the theoretically predicted dependencies for the Rabi oscillations and multiphoton absorption spectra can be observed experimentally for realistic AGNR subject to readily available light fields. The results presented above can be qualitatively extended to the quantum electrodynamic vacuum decay in the presence of strong time-oscillating electric fields and the AGNR can be treated as a condensed matter medium for the study of particle-antiparticle creation processes, induced by the intensive time-dependent electric fields.

## ACKNOWLEDGMENTS

The authors are grateful to S. P. Gavrilov for many useful discussions and valuable comments as well as M. Pyzh for significant assistance in numerical calculations and graphics.

[1] P. R. Wallace, Phys. Rev. **71**, 622 (1947).
[2] A. H. Castro Neto, F. Guinea, N. M. R. Peres, K. S. Novoselov, and A. K. Geim, Rev. Mod. Phys. **81**, 109 (2009).
[3] S. Das Sarma, S. Adam, E. H. Hwang, and E. Rossi, Rev. Mod. Phys. **83**, 407 (2011).
[4] A. H. Castro Neto and A. K. Geim, Science **324**, 1530 (2009).
[5] F. Fillion-Gourdeau, D. Gagnon, C. Lefebvre, and S. MacLean, Phys. Rev. B **94**, 125423 (2016).
[6] D. Allor, T. D. Cohen, and D. A. McGady, Phys. Rev. D **78**, 096009 (2008).
[7] F. Sauter, Zeitschr. f. Physik **73**, 547 (1932).
[8] O. Klein, Z. Phys. **53**, 157 (1929).
[9] J. Schwinger, Phys. Rev. **82**, 664 (1951).
[10] A. I. Nikishov, Nucl. Phys. B **21**, 346 (1970).
[11] T. D. Cohen and D. A. McGady, Phys. Rev. D **78**, 036008 (2008).
[12] N. B. Narozhnyi and A. I. Nikishov, Sov. J. Nucl. Phys. **11**, 596 (1970).
[13] A. I. Nikishov, Sov. Phys. J. Exp. Theor. Physics **30**, 660 (1970).
[14] T. Brezin and C. Itzykson, Phys. Rev. D **2**, 1191 (1970).
[15] V. S. Popov, Sov. Phys. J. Exp. Theor. Physics **34**, 709 (1972).
[16] A. M. Fedotov, E. G. Gelfer, K. Yu. Korolev, and S. A. Smolyansky, Phys. Rev. D **83**, 025011 (2011).
[17] I. Akal, R. Egger, C. Müller, and S. Villalba-Chavez, Phys. Rev. D **99**, 016025 (2019).
[18] L. V. Keldysh, Sov. Phys. J. Exp. Theor. Physics **20**, 1307 (1965).
[19] V. M. Mostepanenko and V. M. Frolov, Sov. J. Nucl. Phys. **19**, 451 (1974).
[20] G. V. Dunne, H. Gies, and R. Schützhold, Phys. Rev. D **80**, 111301(R) (2009).
[21] F. Cooper and E. Mottola, Phys. Rev. D **40**, 456 (1989).
[22] Y. Kluger, J. M. Eisenberg, B. Svetitsky, F. Cooper, and E. Mottola, Phys. Rev. D **45**, 4659 (1992).
[23] R. Brout, S. Massar, R. Parentani, S. Popescu, and Ph. Spindel, Phys. Rev. D **52**, 1119 (1995).
[24] M. Bordag, G. L. Klimchitskaya, U. Mohideen, and V. M. Mostepanenko, *Advances in the Casimir Effect* (Oxford University, Oxford, 2009).
[25] G. L. Klimchitskaya, U. Mohideen, and V. M. Mostepanenko, Rev. Mod. Phys. **81**, 1827 (2009).
[26] G. L. Klimchitskaya and V. M. Mostepanenko, Phys. Rev. D **87**, 125011 (2013).
[27] A. A. Grib, S. G. Mamayev, and V. M. Mostepanenko, *Vacuum Quantum Effects in Strong Fields* (Friedmann Laboratory, St. Petersburg, 1994).
[28] S. P. Gavrilov and D. M. Gitman, Phys. Rev. D **53**, 7162 (1996).
[29] H. Taya, Phys. Rev. Res. **2**, 023257 (2020).
[30] W. H. Furry, Phys. Rev. **81**, 115 (1951).
[31] H. Taya, T. Fujimori, T. Misumi, M. Nitta, and N. Sakai, J. High Energy Phys. 03 (2021) 082.
[32] M. F. Linder, A. Lorke, and R. Schützhold, Phys. Rev. B **97**, 035203 (2018).
[33] L. V. Keldysh, Sov. Phys. J. Exp. Theor. Physics **18**, 253 (1964).
[34] L. D. Landau, Phys. Z. Sowjetunion **2**, 46 (1932).
[35] C. Zener, Proc. R. Soc. London Ser. A **145**, 523 (1934).
[36] I. Akal, R. Egger, C. Müller, and S. Villalba-Chavez, Phys. Rev. D **93**, 116006 (2016).
[37] S. P. Gavrilov, D. M. Gitman, and N. Yokomizo, Phys. Rev. D **86**, 125022 (2012).
[38] H. K. Avetissian, A. K. Avetissian, G. F. Mkrtchian, and Kh. V. Sedrakian, Phys. Rev. B **85**, 115443 (2012).
[39] F. Fillion-Gourdeau and S. MacLean, Phys. Rev. B **92**, 035401 (2015).
[40] D. Gagnon, F. Fillion-Gourdeau, J. Dumont, C. Lefebvre, and S. MacLean, Phys. Rev. B **93**, 205415 (2016).
[41] S. Y. Zhou, G. H. Gweon, A. V. Fedorov, P. N. First, W. A. deHeer, D. H. Lee, F. Guinea, A. H. Castro Neto, A. Lanzara, Nat. Mater. **6**, 770 (2007).
[42] L. Brey and H. A. Fertig, Phys. Rev. B **73**, 235411 (2006).

[43] V. Barone, O. Hod, and G. E. Scuseria, Nano Lett. **6**, 2748 (2006).
[44] L. Yang, M. L. Cohen, and S. G. Louie, Nano Lett. **7**, 3112 (2007).
[45] H. Hsu and L. E. Reichl, Phys. Rev. B **76**, 045418 (2007).
[46] D. Prezzi, D. Varsano, A. Ruini, A. Marini, and E. Molinari, Phys. Rev. B **77**, 041404(R) (2008).
[47] K. Gundra and A. Shukla, Phys. Rev. B **83**, 075413 (2011).
[48] M. Inglot, V. K. Dugaev, J. Berakdar, and J. Barnas', Phys. Rev. B **100**, 165406 (2019).
[49] K. Sasaki, K. Kato, Y. Tokura, K. Oguri, and T. Sogawa, Phys. Rev. B **84**, 085458 (2011).
[50] B. S. Monozon and P. Schmelcher, Phys. Rev. B **86**, 245404 (2012).
[51] L. L. Foldy and S. A. Wouthuysen, Phys. Rev. **78**, 29 (1950).
[52] A. G. Aronov and G. E. Pikus, Sov. Phys. J. Exp. Theor. Physics **24**, 339 (1967).
[53] A. G. Zhilich and B. S. Monozon, Sov. Phys. J. Exp. Theor. Physics **48**, 867 (1978).
[54] L. D. Landau and E. M. Lifshitz, *Quantum Mechanics: Nonrelativistic Theory* (Pergamon, London, 1981).
[55] M. Abramowitz and I. A. Stegun (Eds.), *Handbook of Mathematical Functions* (Dover, New York, 1972).
[56] L. V. Keldysh, Sov. Phys. J. Exp. Theor. Physics **6**, 763 (1958).
[57] N. F. Perel'man, Sov. Phys. J. Exp. Theor. Physics **41**, 822 (1976).
[58] V. A. Kovarsky, N. F. Perelman, and I. Sh. Averbukh, *Multiphoton Processes* (Energoatomizdat, Moscow, 1985), in Russian.
[59] V. S. Popov, Sov. J. Nucl. Phys. **19**, 584 (1974).
[60] S. P. Kim and D. N. Page, Phys. Rev. D **65**, 105002 (2002).
[61] V. S. Popov and M. S. Marinov, Sov. J. Nucl. Phys. **16**, 449 (1973).
[62] F. Hebenstreit, R. Alkofer, and H. Gies, Phys. Rev. D **82**, 105026 (2010).
[63] S. M. Schmidt, D. Blaschke, G. Röpke, S. A. Smolyansky, and A. V. Prozorkevich, Int. J. Mod. Phys. E **07**, 709 (1998).
[64] I. Akal, S. Villalba-Chavez, and C. Müller, Phys. Rev. D **90**, 113004 (2014).
[65] T. C. Adorno, S. P. Gavrilov, and D. M. Gitman, Int. J. Mod. Phys. A **32**, 1750105 (2017).